Optics Letters

All-fiber polarization-maintaining mode-locked laser operated at 980 nm

Svetlana S. Aleshkina,[1] Andrei Fedotov,[2,*] Dmitrii Korobko,[3] Dmitrii Stoliarov,[3] Denis S. Lipatov,[4] Vladimir V. Velmiskin,[1] Valery L. Temyanko,[5] Leonid V. Kotov,[5] Regina Gumenyuk,[2,3] and Mikhail E. Likhachev[1]

[1]Fiber Optics Research Center of the Russian Academy of Sciences, 38 Vavilov Street, 119333 Moscow, Russia
[2]Laboratory of Photonics, Tampere University, Korkeakoulunkatu 3, 33720 Tampere, Finland
[3]Ulyanovsk State University, 42 Leo Tolstoy Street, 432017 Ulyanovsk, Russia
[4]Institute of High Purity Substances of the Russian Academy of Sciences, 49 Tropinin Street, 603950 Nizhny Novgorod, Russia
[5]College of Optical Sciences, University of Arizona, 1630 E. University Blvd, Tucson, Arizona 85721-0094, USA
*Corresponding author: andrei.fedotov@tuni.fi

Received 20 February 2020; accepted 8 March 2020; posted 16 March 2020 (Doc. ID 391193); published 9 April 2020

For the first time, to the best of our knowledge, we present an all-fiber polarization-maintaining passively mode-locked picosecond laser operated at 980 nm. The laser cavity had a ring configuration with a semiconductor saturable absorber mirror as a mode-locking element. As an active medium, we used a specially designed cladding-pumped Yb-doped fiber with reduced cladding-to-core diameter ratio. The laser was self-starting and operated in the net cavity normal dispersion regime, where a spectral profile of the gain medium acted as a filter element. By intracavity spectral filtering, we achieved about 40 dB dominance of the signal wavelength at 980 nm over 1 μm emission in a highly stable picosecond pulsed regime. The corresponding simulation was performed to extend the knowledge about laser operation.

https://doi.org/10.1364/OL.391193

Ytterbium-based lasers operating in a short near-infrared wavelength range are attractive solutions as pump sources for Yb- and Er-doped all-fiber amplification systems and are also extremely promising for frequency conversion. By frequency doubling and quadrupling a 980 nm pulsed laser, highly coherent blue 488 nm and ultraviolet 244 nm radiation can be generated. Nowadays, there is a high demand for such a wavelength for an ever-increasing list of applications such as underwater exploration of marine resources, data transmission, displays, spectroscopy, and biophotonics [1–4]. In this context, compact, powerful all-fiber lasers are of particular interest since they can potentially replace bulky and inefficient argon and excimer lasers.

Although lasing of Yb^{3+} ions has been demonstrated in the broad spectral range from 970 to 1150 nm, the development of a 980 nm laser is not a trivial task. The main difficulty arises from the fact that 980 nm emission of Yb^{3+} ions corresponds to a three-level laser system (which entails high lasing thresholds and requires at least of 50% population inversion), whereas emitting Yb^{3+} ions at 1030 nm corresponds to a much more efficient four-level system.

To mitigate the lasing of Yb^{3+} ions at 1030 nm, special active fiber designs have been proposed as the most effective measure. One approach is to use short highly doped single-mode fiber (SMF) and in-core pumping by single-mode diodes [5–7]. However, the output power of any available single-mode pump sources at 915 nm is limited to a few hundred milliwatts. Therefore, the cladding pump scheme is more beneficial for power scaling. For this approach, a double-clad design with a special gain filtering structure [8] or one with enhanced pump absorption due to the increase in the ratio of the core and cladding diameters have both been demonstrated [9–14]. The fibers with the special gain filtering proved themselves to be the most efficient active medium in high-power continuous-wave (CW) lasers or amplifiers. A record high 151 W in a CW regime was reached using photonics bandgap fiber with enhanced leakage of 1030 nm [8]. The double-clad fiber designs had a large core diameter (more than 20 μm), which resulted in record high output power at 980 nm in the CW regime, although they were not effective for mode-locked seed laser applications. Currently, passive mode locking is the most commonly used method to obtain picosecond pulses at 980 nm wavelength. The first 980 nm picosecond fiber laser that exploited semiconductor saturable absorber mirror (SESAM) was reported by Okhotnikov *et al.* [5]. Later, Zhou *et al.* created a mode-locked laser based on nonlinear polarization evolution [15]. Both lasers included free-space bulk optical elements (diffraction gratings, waveplates, bandpass filters, etc.), which significantly complicated the maintenance of the laser, reducing their reliability and making them cumbersome. On the other hand, the all-fiber configuration of mode-locked picosecond lasers has recently been demonstrated by exploiting non-polarization-maintaining fibers [16]. This approach overcame the complexity of using bulk elements but lacked long-term stability of operation, which is essential for seed lasers in a high-power system. So far, monolithic polarization-maintaining (PM)-type fiber lasers free

of bulk glass components have been demonstrated only with modulated signal or CW operation [17,18].

In this Letter, we demonstrate a robust and compact all-fiber PM picosecond laser based on a cladding-pumped scheme and passively mode locked by the SESAM. The specially designed Yb-doped fiber with a reduced cladding-to-core diameter ratio is used as an effective active medium for 980 nm generation. The laser is designed to operate in an all-normal dispersion regime with the gain medium acting as a spectral filter. The corresponding numerical simulation provides additional details of the laser operation, particularly for spectrum asymmetry due to accumulated third-order dispersion.

The basic schematic for an all-fiber mode-locked ring laser is shown in Fig. 1(a). A mode-locking mechanism was enabled by the specially designed SESAM for operation at 980 nm. The parameters of the SESAM were: saturation fluence 60 $\mu J/cm^2$, modulation depth 9%, and 500 fs of relaxation time. As an active element of the laser, we used 16 cm of Yb-doped all-glass fiber (the fraction of ytterbium oxide in the glass matrix was 0.16 mol%; absorption from the cladding at a pump wavelength of 915 nm was 3.4 dB/m) with a silica cladding reduced to 80 μm [19]. The use of a smaller than conventional cladding diameter compared to conventional fibers (80 μm against 125 μm) while retaining a core diameter typical of SMF with a large-mode area (∼12 μm) results in a reduction of the cladding-to-core ratio. Such a fiber architecture provides higher pump intensity in the Yb-doped core leading to a higher pump absorption rate and, consequently, more efficient generation at 980 nm. The active fiber was designed with a complex Yb-doping profile aimed to increase absorption from the cladding and the complex refractive index profile to preserve single-mode propagation and compatibility with commercially available fibers [Fig. 1(b)]. Being insensitive to the photodarkening effect, a phospho-aluminosilicate glass matrix [20] was used as the basis for the active fiber core. The mode field diameter (MFD_x) of the active fiber was 12 μm, and the MFD_y was 14 μm. The laser cavity was implemented based on a cladding-pumped scheme [Fig. 1(a)]. A commercially available multimode semiconductor diode with a maximum output power of 10 W, emitting at a wavelength of 915 nm, was used as a pump source. To overcome excess cladding losses between the active fiber and the pump combiner (standard pump combiners have a silica cladding diameter of 125–130 μm), we fabricated a special pump combiner with a (2 + 1 in 1) configuration. With this device, the core diameter of the signal fiber was as large as 10 μm, while the silica cladding diameter was as small as 80 μm (pump cladding losses were 0.8 dB; signal core losses at 980 nm were 2.9 dB). The unabsorbed pump power was eliminated from the laser system by a homemade fiber pump stripper [11]. All the laser components were PM, and the fast axis was blocked in a circulator to allow lasing at only one polarization. The mode-locked laser operated in the all-normal dispersion regime, where a narrow gain of Yb at 980 nm acted as a spectral filter, which is essential for stable operation in this regime.

It is well known that there are two principle difficulties that inhibit laser implementation at 980 nm (based on Yb-doped fibers): high lasing thresholds for amplification at 980 nm (due to the three-level laser scheme and the overlapping of the emission and absorption cross sections of Yb-ions at 980 nm) and low population inversion required for lasing at wavelengths longer than 1000 nm (due to four-level and/or quasi-three-level

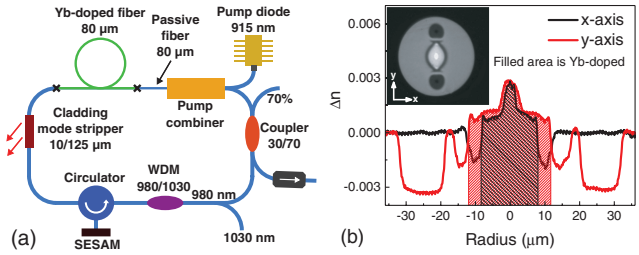

Fig. 1. (a) Scheme of 980 nm mode-locked (ML) fiber laser. (b) Refractive index profile of Yb-doped fiber. Inset: facet image of the active fiber.

laser schemes and low value of the absorption cross section versus the emission cross section). To overcome these problems, we applied additional measures. First, to evacuate most of the emission from the laser cavity at 1030 nm, we introduced into the scheme a 980/1030 wavelength-division multiplexer (WDM) filter. However, even though the Yb^{3+} emission cross section in the region close to 1000 nm was small enough, the generation of wavelengths located at the transmission boundary of the 980/1030 WDM filter prevented amplification at a wavelength of 980 nm. Therefore, to provide reliable generation only at a wavelength of 980 nm, we had to significantly decrease the active fiber length relative to the optimal one (to 16 cm versus 45 cm in the amplifier [19]). The shorter fiber length allowed it to avoid amplification of an undesirable wavelength of 1 mm, belonging to the edge of WDM 980/1030, and create a condition for uniform distribution of the population inversion close to 100% along the active fiber length (providing maximum gain at 980 nm). At the same time, we established the condition when the gain at wavelengths of 1000–1080 nm was so small that emission at 1000–1080 nm could not have an essential influence on the population inversion and could not provide radiation generation. In addition, intracavity losses were increased by using a 30/70 coupler, where 70% of the total power was extracted from the ring laser system. To prevent unwanted back reflection from the free tail of the 30/70 coupler for a signal wavelength at 980 nm and parasitic lasing at 1030 nm, an isolator adapted to operate at both wavelengths with maximum isolation at 1030 nm was used.

The laser turned on in CW operation at a pump power of ∼3.2 W. The pulse operation was self-starting for pump powers above 4.6 W, with an output power of 3.25 mW. The main reason for low total efficiency of our laser relies on high lasing thresholds connected mainly with usage of a short length of the large-mode-area active fiber. Figure 2(a) illustrates an optical spectrum with a steep-edge shape, which is typical for an all-normal dispersion regime. The spectrum was normalized to the spontaneous emission profile. The figure reveals dual-wavelength operation with the spectra being positioned close to each other. One spectrum was centralized at 976.2 nm, and its full width at half bandwidth was 0.44 nm. The central wavelength of the second spectrum was 977.25 nm, and its corresponding full width at half maximum was 0.22 nm. Both spectra together occupied the whole gain bandwidth [Fig. 2(a)]. The dominant peak formed at the left edge of the longer wavelength spectrum was formed mostly due to the highest gain value at this wavelength. The signal-to-amplified spontaneous emission (ASE) ratio of each spectrum was almost

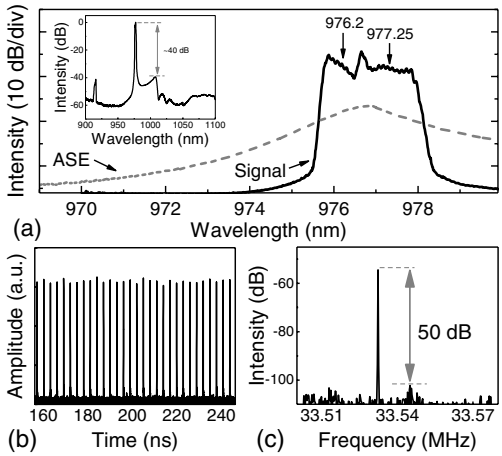

Fig. 2. (a) Optical spectrum of the output signal and gain spectral profile (resolution of 0.05 nm). Inset: optical spectrum covering the measuring region from 900 to 1100 nm (resolution of 0.5 nm). (b) RF spectrum of the mode-locked laser. Inset: oscilloscope trace and autocorrelation function.

as high as 26 dB indicating efficient laser operation at the signal wavelength. In the laser, the active fiber played a dual role: it acted as a gain medium and as a spectral filter, thus allowing the number of required components in the cavity to be minimized. As can be seen in Fig. 2(a) (inset), parasitic lasing at bands over 1000 nm was effectively suppressed: signal-to-noise ratio was about 40 dB. The peak at 915 nm identified the residual unabsorbed pump captured by the active core NA and propagating in the cavity. The shape of the spectrum at wavelengths longer than 1 μm corresponds to the transmission spectrum of WDM 980/1030 used in the scheme. The pulse repetition rate was 33.4 MHz, which corresponded to the round-trip time of the cavity [Fig. 2(b)]. Signal-to-noise ratio measured in the radio frequency range was more than 50 dB [Fig. 2(c)] with the noise level recorded at −110 dB. The line width was ∼1 kHz (the resolution limit of the RF analyzer), which indicates the extremely high stability of this mode-locked laser.

The measured autocorrelation trace is presented in Fig. 3(b). It was best when fitted with a sech^2 profile, and pulse duration was estimated to be as long as 9.5 ps. We assumed that this pulse corresponded to the narrowest spectrum whose time-bandwidth product was 0.66. External pulse compression by a pair of gratings prevented a transform-limited pulse, which might be due to the nonlinear nature of the residual chirp. It was not possible to measure the pulse corresponding to the second (broader) spectrum by adjusting the wavelength of the autocorrelator, probably due to the two spectra being too close to each other and the long pulse duration.

We further optimized the cavity by replacing the output coupler with a higher coupling ratio of 80%. As in the previous case, most of the generated signal was extracted from the laser cavity. It helped to expand the single spectrum covering the whole gain bandwidth [Fig. 3(a)]. The full width at half maximum of the spectrum was 1.75 nm. The measured pulse function is shown in Fig. 3(b). The pulse duration was 7.6 ps resulting in a time-bandwidth product equal to 4.18. The corresponding transform-limited pulses were sub-ps (if the hyperbolic approximation is accepted). The asymmetry of the spectrum can be attributed to the accumulated third-order dispersion

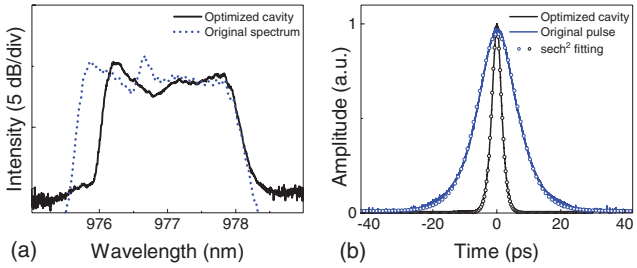

Fig. 3. (a) Optical spectrum and (b) autocorrelation for the optimized cavity with 80/20 and 70/30 couplers inside the cavity.

of the cavity where the majority corresponded to the SESAM according to the simulation results, which are described below.

The laser configuration used in the simulation was identical to the one shown in Fig. 1(a). Signal propagation in active fiber length L_g is described by the Ginzburg–Landau equation for complex amplitude [21]:

$$\frac{\partial A}{\partial z} - i\frac{\beta_{2g}}{2}\frac{\partial^2 A}{\partial t^2} - i\frac{\beta_{3g}}{6}\frac{\partial^3 A}{\partial t^3} - i\gamma_g |A|^2 A = \frac{gA}{2} + \frac{\beta_{2f}}{2}\frac{\partial^2 A}{\partial t^2}. \tag{1}$$

Here $A(z, t)$ is the slowly changing field amplitude, z is a coordinate along the cavity, t is time in an accompanying coordinate system, β_{2g}, β_{3g} are the values of the dispersion of group velocities (GVD) and the third-order dispersion (TOD) of fiber, and γ_g is Kerr nonlinearity. Equation (1) differs from the nonlinear Schrödinger equation (NSE) by (i) the presence of the term $\beta_{2f} = g/\Omega_g^2$, describing a parabolic spectrum gain with the parameter Ω_g, which determines the gain line width (in c^{-1}); (ii) the fact that the gain g due to saturation, depends on the length:

$$g(z, t) = g(z) = g_0\left(1 + \frac{\int_0^{\tau_{\mathrm{win}}} |A(z, t)|^2 \mathrm{d}t}{E_g}\right)^{-1}. \tag{2}$$

Here g_0 is the small signal gain, E_g is gain saturation energy, and τ_{win} is simulation window sizes. Signal propagation in a passive SMF of length L is described by the NSE

$$\frac{\partial A}{\partial z} - i\frac{\beta_2}{2}\frac{\partial^2 A}{\partial t^2} - i\frac{\beta_3}{6}\frac{\partial^3 A}{\partial t^3} - i\gamma |A|^2 A = 0, \tag{3}$$

where β_2, β_3, γ are parameters of GVD, TOD, and Kerr nonlinearity of a SMF. Equations (1) and (3) are simulated by the split-step Fourier (SSF) method in the simulation window of ∼153 ps, including 2^{10} points. We exploit a standard rate equation to simulate the response of the SESAM $\alpha(t)$:

$$\frac{d\alpha}{dt} = \frac{\alpha_0 - \alpha}{\tau_s} - \frac{\alpha |A(z, t)|^2}{E_s}, \tag{4}$$

where α_0 is modulation depth, τ_s is relaxation time, and E_s is saturation energy of the SESAM. The response of the SESAM is inhomogeneous in the spectrum so its dispersion parameters are introduced to take this effect into account. β_{2r}, β_{3r} correspond to the GVD and TOD of the SESAM, respectively. As a result, the response of the SESAM is written in the form of two equations:

Table 1. Parameters of the Ring Resonator

Parameter	Value	Parameter	Value
γ, γ_g ($W^{-1}\,m^{-1}$)	0.0015	E_g (nJ)	1
β_2, β_{2g} ($ps^2\,m^{-1}$)	0.05	Ω_g (ps^{-1})	0.25 (~ 4 nm at 980 nm)
β_3, β_{3g} ($ps^3\,m^{-1}$)	0.001	τ_s (ps)	0.5
g_0 (m^{-1})	1.5	α_0	0.15
β_{2r} (ps^2)	−0.002	E_s (pJ)	50
β_{3r} (ps^3)	0.1	$L; L_g$ (m)	5.7; 0.3

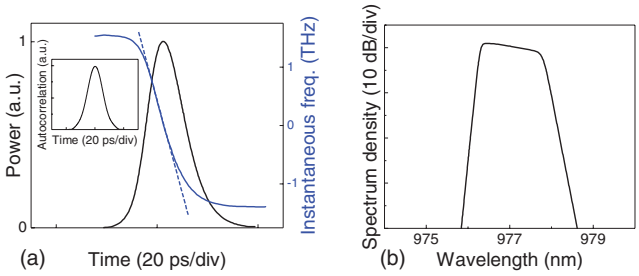

Fig. 4. Envelope of the generated pulse and its frequency modulation. The dashed line shows a linear approximation of frequency modulation. The inset shows the (a) autocorrelation of the generated pulse and the (b) simulated spectrum of the generated pulse.

$$A'(t) = (1-\alpha)A_{\text{in}}(t),$$

$$A_{\text{out}}(\omega) = A'(\omega)\exp\left(-i\left(\frac{\beta_{2r}}{2}\omega^2 + \frac{\beta_{3r}}{6}\omega^3\right)\right). \quad (5)$$

The accumulated loss in the cavity was performed using the output coupler transfer function $A' = A \cdot B$, where $B = 0.55$. The remaining values of the parameters of the ring resonator are given in Table 1.

A low-amplitude Gaussian noise was defined as the initial condition. At the specified laser parameters, the laser after ~100 passes of the cavity transits into the stationary generation of a single pulse. The simulated laser output parameters are presented in Fig. 4. As can be seen, the spectrum and autocorrelation obtained during the simulation are close to those obtained in the experiment (Fig. 3). The pulse has a significant frequency modulation, which is a characteristic feature of lasers with net cavity normal dispersion. A significant amount of the TOD of the resonator, the main part of which consists of the TOD of the SESAM, leads to a noticeable asymmetry of frequency modulation, which, accordingly, causes asymmetry of the pulse envelope and spectral density.

In conclusion, we are the first to demonstrate the all-fiber PM picosecond mode-locked laser operated at a highly demanding 980 nm wavelength range. The specially designed Yb-doped double-clad fiber with a reduced core-to-cladding diameter ratio allowed the implementation of an efficient clad-pumping scheme. The laser cavity was composed to operate in an all-normal dispersion regime with a novel approach in which the spectral profile of the gain medium acts as an essential filtering element to stabilize the mode-locked operation. We achieved around 40 dB of the 980 nm signal dominance over 1 μm emissions in a highly stable picosecond pulsed regime. Future work will focus on the assembly of a master oscillator power amplifier/chirped pulse amplification system, followed by frequency doubling to obtain 490 nm.

Funding. Academy of Finland (320165, 323268); Russian Science Foundation (18-79-00187, 19-72-10037).

Disclosures. The authors declare no conflicts of interest.

REFERENCES

1. T.-C. Wu, Y.-C. Chi, H.-Y. Wang, C.-T. Tsai, and G.-R. Lin, Sci. Rep. **7**, 40480 (2017).
2. Y.-F. Huang, Y.-C. Chi, H.-Y. Kao, C.-T. Tsai, H.-Y. Wang, H.-C. Kuo, S. Nakamura, D.-W. Huang, and G.-R. Lin, Sci. Rep. **7**, 10478 (2017).
3. O. Maragò, B. Fazio, P. Gucciardi, and E. Arimondo, Appl. Phys. B **77**, 809 (2003).
4. Y. Wang, X. Wu, J. Chen, R. Amin, M. Lu, B. Bhayana, J. Zhao, C. K. Murray, M. R. Hamblin, D. C. Hooper, and T. Dai, J. Infect. Dis. **213**, 1380 (2016).
5. O. G. Okhotnikov, L. Gomes, N. Xiang, T. Jouhti, and A. B. Grudinin, Opt. Lett. **28**, 1522 (2003).
6. L. A. Gomes, L. Orsila, T. Jouhti, and O. G. Okhotnikov, IEEE J. Sel. Top. Quantum Electron. **10**, 129 (2004).
7. C. Bartolacci, M. Laroche, H. Gilles, S. Girard, T. Robin, and B. Cadier, in *Advances in Optical Materials*, OSA Technical Digest (Optical Society of America, 2011), paper ATuB9.
8. W. Li, T. Matniyaz, S. Gafsi, M. T. Kalichevsky-Dong, T. W. Hawkins, J. Parsons, G. Gu, and L. Dong, Opt. Express **27**, 24972 (2019).
9. K. H. Ylä-Jarkko, R. Selvas, D. B. S. Soh, J. K. Sahu, C. A. Codemard, J. Nilsson, S. A. Alam, and A. B. Grudinin, in *Advanced Solid-State Photonics*, OSA Trends in Optics and Photonics (Optical Society of America, 2003), paper 103.
10. D. B. S. Soh, C. Codemard, J. K. Sahu, J. Nilsson, V. Philippov, C. Alegria, and Y. Jeong, in *Advanced Solid-State Photonics*, OSA Technical Digest (Optical Society of America, 2004), paper MA3.
11. S. S. Aleshkina, T. A. Kochergina, K. K. Bobkov, L. V. Kotov, M. M. Bubnov, J. Park, and M. E. Likhachev, in *Conference on Lasers and Electro-Optics (CLEO)*, OSA Technical Digest (Optical Society of America, 2016), paper JTu5A.106.
12. S. S. Aleshkina, A. E. Levchenko, O. I. Medvedkov, K. K. Bobkov, M. M. Bubnov, D. S. Lipatov, A. N. Guryanov, and M. E. Likhachev, IEEE Photon. Technol. Lett. **30**, 127 (2018).
13. F. Röser, C. Jauregui, J. Limpert, and A. Tünnermann, Opt. Express **16**, 17310 (2008).
14. J. Boullet, Y. Zaouter, R. Desmarchelier, M. Cazaux, F. Salin, J. Saby, R. Bello-Doua, and E. Cormier, Opt. Express **16**, 17891 (2008).
15. Y. Zhou, Y. Dai, J. Li, F. Yin, J. Dai, T. Zhang, and K. Xu, Laser Phys. Lett. **15**, 075107 (2018).
16. P.-X. Li, Y.-F. Yao, J.-J. Chi, H.-W. Hu, G.-J. Zhang, B.-X. Liang, M.-M. Zhang, C.-M. Ma, and N. Su, Chin. Phys. B **25**, 084207 (2016).
17. V. Khitrov, D. Machewirth, B. Samson, and K. Tankala, "Proc. SPIE **6102**, 610222 (2006).
18. J. Wu, X. Zhu, H. Wei, K. Wiersma, M. Li, J. Zong, A. Chavez-Pirson, V. Temyanko, L. J. LaComb, R. A. Norwood, and N. Peyghambarian, Opt. Lett. **43**, 951 (2018).
19. S. S. Aleshkina, D. S. Lipatov, T. A. Kochergina, V. V. Velmiskin, V. L. Temyanko, L. V. Kotov, T. L. Bardina, M. M. Bubnov, A. N. Guryanov, and M. E. Likhachev, Quantum Electron. **49**, 919 (2019).
20. M. E. Likhachev, S. S. Aleshkina, A. V. Shubin, M. M. Bubnov, E. M. Dianov, D. S. Lipatov, and A. N. Guryanov, in *CLEO/Europe and EQEC 2011 Conference Digest*, OSA Technical Digest (Optical Society of America, 2011), paper CJ_P24.
21. G. P. Agrawal, *Nonlinear Fiber Optics, Optics and Photonics*, 2nd ed. (Academic, 1995).